

DYNAMIC SIMULATION OF A SPATIAL 3-DOF TENSEGRITY MECHANISM

MARC ARSENAULT

Département de Génie Mécanique
Université Laval
Québec, Québec, Canada, G1K 7P4
marc.arsenault.1@ulaval.ca

CLÉMENT M. GOSSELIN*

Département de Génie Mécanique
Université Laval
Québec, Québec, Canada, G1K 7P4
gosselin@gmc.ulaval.ca

Résumé

Les mécanismes tensegrités sont avantagés par leur utilisation judicieuse de câbles et de ressorts, ce qui mène à une réduction considérable de l'inertie de leurs pièces mobiles. En conséquence, ces mécanismes pourraient éventuellement devenir des alternatives attrayantes pour remplacer les mécanismes conventionnels dans certains types d'applications. Toutefois, la présence de degrés de liberté non-contraints dans les mécanismes tensegrités mène à un comportement dynamique qui ne peut pas être commandé directement par les actionneurs. Dans cet ouvrage, le modèle dynamique d'un nouveau mécanisme tensegrité spatial à trois degrés de liberté est développé en utilisant la formulation Lagrangienne. Par la suite, les équations de mouvement du mécanisme sont résolues pour simuler son mouvement entre deux configurations d'équilibre. Puisque le mécanisme est assujéti à des contraintes géométriques non-linéaires holonomes, ces dernières doivent être considérées pendant le calcul de la solution du problème dynamique direct. Il est démontré que l'utilisation d'amortisseurs en parallèle avec les ressorts du mécanisme ne parvient pas à dissiper l'énergie de ce dernier de manière efficace.

Abstract

Tensegrity mechanisms have the advantage of being relatively lightweight due to their extensive use of cables and springs. As such, they have the potential of being an attractive alternative to conventional mechanisms in certain application environments. However, the presence of unconstrained degrees of freedom in tensegrity mechanisms leads to a dynamic behaviour which cannot be directly controlled with the actuators. In this work, the dynamic model of a novel spatial three-degree-of-freedom (3-DOF) tensegrity mechanism is developed using the Lagrangian formulation. The resulting equations of motion are then solved to simulate the mechanism's motion between equilibrium configurations. Since the mechanism is subjected to holonomic nonlinear geometrical constraints, these must be considered during the solution of its forward dynamic problem. It is seen that the use of damping in the springs is not very efficient in dissipating the mechanism's energy during motion.

* Author to whom correspondence should be addressed.

1 Introduction

Tensegrity systems are defined as structures or mechanisms whose components are subjected to either traction or compression forces in all possible configurations. The use of springs or cables for the tension components allows for a significant reduction of the mass of such systems. Consequently, tensegrity mechanisms have recently been introduced as potential alternatives to heavier conventional mechanisms for certain types of applications.

Research on tensegrity systems dates back to the middle of the twentieth century when Buckminster Fuller, inspired by artist Kenneth Snelson’s novel sculptures, introduced the word *tensegrity* as a combination of the words *tension* and *integrity* [1]. A detailed history of these systems is given by Motro [2]. Research on tensegrity mechanisms is much more recent [3–7]. Among the proposed mechanisms, a flight simulator [8], a space telescope [9] as well as a tensegrity sensor [10] are found.

The object of this paper is to analyze the dynamics of a spatial 3-DOF tensegrity mechanism. The dynamic model of the mechanism is first developed using the Lagrangian formulation. Afterwards, the forward dynamic problem is solved in order to analyze the behaviour of the mechanism in motion. This leads to an important observation pertaining to the mechanism’s damping.

2 Geometrical Description

A diagram of the spatial 3-DOF tensegrity mechanism is shown in Figure 1a. It consists of twelve components in traction of which nine are springs joining node pairs A_iA_j and A_iC_j ($i = 1, 2, 3, j = 1, 2, 3$ and $i \neq j$). The springs have stiffness K , lengths l_k ($k = 1, 2, \dots, 9$) and zero free lengths. This last hypothesis is not problematic since virtual zero free length springs can be created by extending the actual springs beyond their attachment points [11]. Examples of this are given in [12]. The remaining three components in traction are cables (*i.e.* elements that cannot resist compressive forces) of length L that join node pairs C_iC_j . Typically, in the tensegrity system architecture from which the mechanism

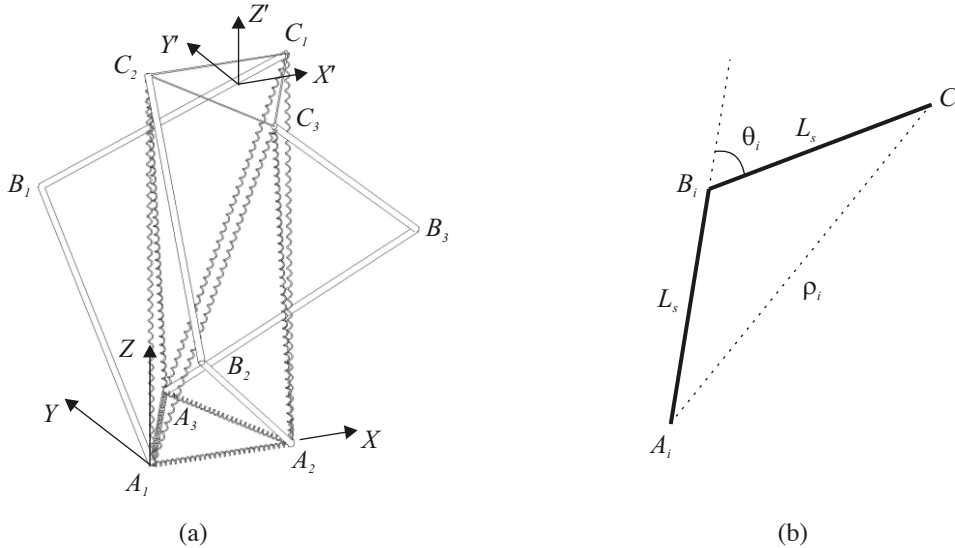


Figure 1: (a) Spatial 3-DOF tensegrity mechanism. (b) Virtual prismatic actuator.

is developed, the components joining node pairs A_iC_i are struts. For the mechanism studied here, it is sought to vary the distance between nodes A_i and C_i with prismatic actuators. However, since such actuators would interfere with each other due to the mechanism architecture, virtual prismatic actuators are used. Node A_i is thus linked to node C_i with a leg consisting of two struts of length L_s . The proximal

strut is attached to node A_i with a universal joint while the proximal and distal struts are joined together by a revolute actuator. Furthermore, spherical joints are used to connect the cables to the distal struts at nodes C_i . By modifying the position of the actuator (θ_i), the effective distance (ρ_i) between nodes A_i and C_i can be varied. The relation between θ_i and ρ_i can easily be computed using the law of cosines as follows (see Figure 1b):

$$\rho_i = \sqrt{2}L_s\sqrt{1 + \cos\theta_i} \quad (1)$$

The actual revolute actuator can be located on the mechanism base and combined with a cable-pulley system to control the angle between the proximal and distal struts thus reducing the inertia of the moving parts. Furthermore, it should be noted here that, because of the architecture of the virtual prismatic actuators, the mechanism deviates slightly from the tensegrity system definition since its struts are not axially loaded.

A fixed reference frame XYZ is defined as being located at node A_1 with its X axis directed towards node A_2 and its Z axis perpendicular to the plane formed by nodes A_i . Similarly, a mobile reference frame $X'Y'Z'$ is defined as being attached to the geometrical centre of nodes C_i with the X' axis parallel to the line formed by nodes C_1 and C_2 and the Z' axis perpendicular to the plane formed by nodes C_i .

Reference frames $x_{r_i}y_{r_i}z_{r_i}$ are attached to the i^{th} leg as shown in Figure 2 ($r = 1, 2, 3, 4$). The rotation matrix bringing frame $(r)_i$ into frame $(r + 1)_i$ is given by:

$$\mathbf{Q}_{r_i} = \begin{bmatrix} \cos \delta_{r_i} & -\cos \gamma_{r_i} \sin \delta_{r_i} & \sin \gamma_{r_i} \sin \delta_{r_i} \\ \sin \delta_{r_i} & \cos \gamma_{r_i} \cos \delta_{r_i} & -\sin \gamma_{r_i} \cos \delta_{r_i} \\ 0 & \sin \gamma_{r_i} & \cos \gamma_{r_i} \end{bmatrix} \quad (2)$$

while the vector linking the origin of frame $(r)_i$ to the origin of frame $(r + 1)_i$ is expressed as:

$$\mathbf{d}_{r_i} = [e_{r_i} \cos \delta_{r_i}, e_{r_i} \sin \delta_{r_i}, h_{r_i}]^T \quad (3)$$

The parameters appearing in Eqs. (2) and (3) are defined in Table 1 for the mechanism's i^{th} leg. Angles α_i and β_i correspond to the rotation of the universal joint located at node A_i . The positions of nodes A_i , B_i and C_i in the fixed reference frame (XYZ) are represented by vectors \mathbf{a}_i , \mathbf{b}_i and \mathbf{c}_i , respectively. Whereas node A_1 is fixed relative to frame XYZ , node A_2 is free to translate along the X axis while node A_3 may move in the XY plane. Vectors \mathbf{a}_i thus become:

$$\mathbf{a}_1 = [0, 0, 0]^T \quad \mathbf{a}_2 = [\mu_1, 0, 0]^T \quad \mathbf{a}_3 = [\mu_2, \mu_3, 0]^T \quad (4)$$

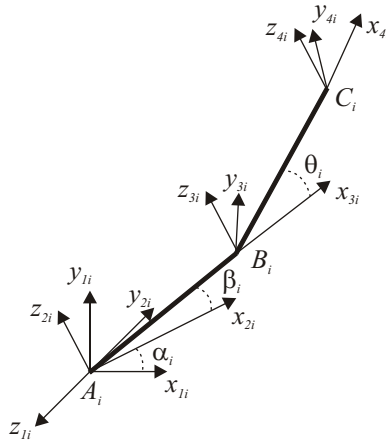


Figure 2: Definition of local reference frames attached to the i^{th} leg.

r	e_{r_i}	h_{r_i}	γ_{r_i}	δ_{r_i}
1	0	0	$-\frac{\pi}{2}$	α_i
2	L_s	0	0	β_i
3	L_s	0	0	θ_i

Table 1: Parameters for the i^{th} leg.

where the lengths defined by μ_i are unactuated. Referring to Figure 1a, vectors \mathbf{b}_i and \mathbf{c}_i can be computed according to the definitions provided in Eqs. (2) and (3) as follows:

$$\mathbf{b}_i = \mathbf{a}_i + \mathbf{R}_i(\mathbf{d}_{1_i} + \mathbf{Q}_{1_i}\mathbf{d}_{2_i}) \quad (5)$$

$$\mathbf{c}_i = \mathbf{a}_i + \mathbf{R}_i[\mathbf{d}_{1_i} + \mathbf{Q}_{1_i}(\mathbf{d}_{2_i} + \mathbf{Q}_{2_i}\mathbf{d}_{3_i})] \quad (6)$$

where \mathbf{R}_i , the rotation matrix bringing the fixed reference frame XYZ in an orientation parallel to frame $x_{1_i}y_{1_i}z_{1_i}$, is expressed as:

$$\mathbf{R}_i = \begin{bmatrix} \cos \zeta_i & 0 & \sin \zeta_i \\ \sin \zeta_i & 0 & -\cos \zeta_i \\ 0 & 1 & 0 \end{bmatrix} \quad (7)$$

with $\zeta_1 = \pi/6$, $\zeta_2 = 5\pi/6$ and $\zeta_3 = -\pi/2$. The mechanism's input vector is:

$$\boldsymbol{\psi} = [\theta_1, \theta_2, \theta_3]^T \quad (8)$$

The application of the Tchebychev-Grübler-Kutzbach mobility formula to the mechanism (the springs need not be considered for this analysis while the cables can be considered to be rigid links) shows that the mechanism has a total of nine degrees of freedom. As a consequence, when the revolute actuators are locked, the mechanism still has six unconstrained degrees of freedom. These are represented here by the following vector of coordinates:

$$\mathbf{q} = [\mu_1, \mu_2, \mu_3, \alpha_1, \beta_1, \alpha_2, \beta_2, \alpha_3, \beta_3]^T \quad (9)$$

of which three are superfluous. In addition to vectors $\boldsymbol{\psi}$ and \mathbf{q} , the following three geometrical constraints associated with the lengths of the cables must also be satisfied in order to completely define the mechanism's configuration:

$$\phi_i = (\mathbf{c}_i - \mathbf{c}_j)^T(\mathbf{c}_i - \mathbf{c}_j) - L^2 = 0 \quad i, j = 1, 2, 3, \quad i \neq j \quad (10)$$

When the actuators are locked, the need for the potential energy stored in the springs to be minimized leads to a unique static equilibrium. By modifying the positions of the actuators, three of the mechanism's six unconstrained degrees of freedom can be controlled. In this work, these are chosen as the position coordinates of the geometric centre of nodes C_i relative to the fixed base which can be represented by the following vector expressing the position of the origin of reference frame $X'Y'Z'$ in frame XYZ :

$$\mathbf{x} = [x, y, z]^T \quad (11)$$

This vector becomes the output of the mechanism. Finally, it should be noted that the stiffnesses of the struts and cables are assumed to be infinite relative to those of the springs. Furthermore, the decision of using springs or cables for each of the tension elements is made with the goal of allowing the mechanism to adapt in order to maintain its tensegrity properties as it moves between equilibrium configurations while also fixing the lengths of a minimal amount of elements so that the equilibrium for a given set of actuator positions is unique.

3 Dynamic Model

It was mentioned in Section 2 that the spatial 3-DOF tensegrity mechanism has unconstrained degrees of freedom. In spite of this, when the actuators are locked, the minimization of the potential energy stored in the mechanism's springs leads to a unique equilibrium configuration. However, when the mechanism is in movement, its configuration is free to change under the influence of inertial loads. For this reason, the analysis of the mechanism's dynamics is essential.

3.1 Hypotheses

In order to develop a model of the mechanism's dynamics, the following hypotheses are made:

- The springs and cables are massless.
- Each strut is modelled as a thin, straight rod of mass m and moment of inertia $I_s = \frac{1}{12}mL_s^2$ about axes passing through its centre of mass and perpendicular to its central axis (the central axis links nodes A_i and B_i for the proximal strut and nodes B_i and C_i for the distal one). The inertia about the central axis is assumed to be zero.
- The joints and the actuators are frictionless.
- The springs are linearly damped with damping coefficient c_d .
- Gravity is neglected.

At first glance, the assumption that gravitational forces are absent seems unrealistic. However, as proposed in [13], gravitational forces associated with the weights of the struts can be compensated using static balancing techniques thus leading to considerable simplifications in the mechanism analysis.

3.2 Equations of Motion

As it was stated in Section 2, vectors $\boldsymbol{\psi}$ and \boldsymbol{q} are both needed to completely define the configuration of the mechanism in the general case. As a result of this, the $N \times 1$ vector of generalized coordinates used for the development of the dynamic model is defined as follows:

$$\boldsymbol{u} = [\boldsymbol{q}^T, \boldsymbol{\psi}^T]^T \quad (12)$$

The equations of motion of the mechanism are developed here using the well-known Lagrangian formulation, namely:

$$\frac{d}{dt} \frac{\partial T}{\partial \dot{\boldsymbol{u}}} - \frac{\partial T}{\partial \boldsymbol{u}} + \frac{\partial U}{\partial \boldsymbol{u}} = \boldsymbol{f}_d + \boldsymbol{\Lambda} \boldsymbol{\tau} \quad (13)$$

In the above expression, T is the kinetic energy of the mechanism expressed as follows:

$$T = \frac{1}{2}m \sum_{i=1}^3 (\dot{\boldsymbol{p}}_{p_i}^T \dot{\boldsymbol{p}}_{p_i} + \dot{\boldsymbol{p}}_{d_i}^T \dot{\boldsymbol{p}}_{d_i}) + \frac{1}{2} \sum_{i=1}^3 (\boldsymbol{\omega}_{p_i}^T \mathbf{I} \boldsymbol{\omega}_{p_i} + \boldsymbol{\omega}_{d_i}^T \mathbf{I} \boldsymbol{\omega}_{d_i}) \quad (14)$$

where \boldsymbol{p}_{p_i} and \boldsymbol{p}_{d_i} , the position vectors of the centres of mass of the i^{th} proximal and distal struts, respectively, are:

$$\boldsymbol{p}_{p_i} = \frac{\boldsymbol{a}_i + \boldsymbol{b}_i}{2} \quad \boldsymbol{p}_{d_i} = \frac{\boldsymbol{b}_i + \boldsymbol{c}_i}{2} \quad (15)$$

Furthermore, $\boldsymbol{\omega}_{p_i}$ and $\boldsymbol{\omega}_{d_i}$, representing the angular velocities of the i^{th} proximal and distal struts, respectively, along reference frames attached to their centres of mass with X axes directed along the struts, can be expressed as:

$$\boldsymbol{\omega}_{p_i} = [\sin \beta_i \dot{\alpha}_i, \cos \beta_i \dot{\alpha}_i, \dot{\beta}_i]^T \quad (16)$$

$$\boldsymbol{\omega}_{d_i} = [\sin(\beta_i + \theta_i)\dot{\alpha}_i, \cos(\beta_i + \theta_i)\dot{\alpha}_i, \dot{\beta}_i + \dot{\theta}_i]^T \quad (17)$$

while \mathbf{I} is the inertia matrix of the struts:

$$\mathbf{I} = I_s \begin{bmatrix} 0 & 0 & 0 \\ 0 & 1 & 0 \\ 0 & 0 & 1 \end{bmatrix} \quad (18)$$

Also from Eq. (13), U is the potential energy stored in the mechanism's springs:

$$U = \frac{1}{2}K \sum_{k=1}^9 l_k^2 \quad (19)$$

while \mathbf{f}_d is a vector of dissipative forces whose n^{th} element ($n = 1, 2, \dots, N$) is expressed as:

$$f_{d_n} = -c_d \sum_{k=1}^9 \dot{l}_k \frac{\partial l_k}{\partial u_n} \quad (20)$$

where \dot{l}_k is the time rate of change of the length of the k^{th} spring and u_n is the n^{th} element of vector \mathbf{u} . Finally, $\boldsymbol{\tau}$, the vector of actuator torques, is expressed as $\boldsymbol{\tau} = [\tau_1, \tau_2, \tau_3]^T$ while:

$$\boldsymbol{\Lambda} = \begin{bmatrix} \mathbf{0}_{6 \times 3} \\ \mathbf{1}_3 \end{bmatrix} \quad (21)$$

where $\mathbf{0}_{6 \times 3}$ is a 6×3 zero matrix and $\mathbf{1}_3$ is the 3×3 identity matrix. Substituting the above definitions in Eq. (13) yields the equations of motion of the mechanism:

$$\mathbf{M}\ddot{\mathbf{u}} + \mathbf{V}(\dot{\mathbf{u}}, \mathbf{u}) + \mathbf{G}(\mathbf{u}) = \boldsymbol{\Lambda}\boldsymbol{\tau} \quad (22)$$

where \mathbf{M} is the $N \times N$ generalized inertia matrix, $\mathbf{V}(\dot{\mathbf{u}}, \mathbf{u})$ is the $N \times 1$ vector of non-linear inertial effects and dissipative forces, and $\mathbf{G}(\mathbf{u})$ is the $N \times 1$ vector of generalized forces due to the potential energy in the springs.

4 Simulation

In order to study the behaviour of the mechanism as it is moved from one equilibrium configuration to another, its forward dynamic problem must be solved. However, as it will be seen, this is not a straightforward process for the mechanism considered here since it is subjected to nonlinear geometrical constraints.

4.1 Solving the Forward Dynamic Problem of Constrained Mechanisms

The spatial 3-DOF tensegrity mechanism can be considered as a closed-chain mechanism. As such, the mechanism's legs can be seen as independent open-loop mechanisms that are subjected to loop-closure equations. This was introduced in Section 2 where the configurations of each of the mechanism's legs were specified using vectors $\boldsymbol{\psi}$ and \mathbf{q} to which holonomic geometrical constraints (Eq. (10)) associated with the cable lengths were added to ensure loop-closure. Ideally, these constraints would be solved for the superfluous coordinates in terms of a set of independent generalized coordinates. These independent coordinates could then be used to develop the dynamic model of the mechanism. However, since the constraints are nonlinear at the position level, this is not possible.

By developing the dynamic model of the mechanism using \mathbf{u} as the vector of generalized coordinates, the equations of motion obtained in Eq. (22) represent a system of 12 nonlinear ordinary differential

equations in 12 unknowns whereas the mechanism only has nine degrees of freedom. As a consequence, the geometrical constraints must be considered along with the equations of motion in order to solve the mechanism's dynamics. This can usually be done using one of two general approaches. The first of these consists in using the constraint equations in order to project the original dynamic model into a minimum set of equations of motion. However, this task can be quite cumbersome in some cases. Furthermore, the resulting set of equations is still dependent at the position level (and in some cases also at the velocity level) on the original set of superfluous coordinates. The second approach consists in solving the dynamics using the original superfluous set of coordinates while simultaneously ensuring that the constraint equations are satisfied. Several methods available to do this are described in [14]. Among these, perhaps one of the best known is based on the use of Lagrange multipliers in order to obtain explicit expressions for the forces associated with the constraints which can then be added to the original equations of motion. This method will now be detailed.

Based on differential variational principles [14], Eq. (22) can be rewritten in the following form:

$$\delta \mathbf{u}^T (\mathbf{M}\ddot{\mathbf{u}} + \mathbf{V}(\dot{\mathbf{u}}, \mathbf{u}) + \mathbf{G}(\mathbf{u}) - \mathbf{\Lambda}\boldsymbol{\tau} - \mathbf{F}) = \mathbf{0} \quad (23)$$

where a vector of constraint forces (\mathbf{F}) has been added and where $\delta \mathbf{u}$ is a vector of kinematic variations (*e.g.* virtual displacements) associated with the parameters used to represent the configuration of the mechanism. If a vector of kinematic variations compatible with the constraints, defined as $\delta \mathbf{u}_c$, can be found in some way then:

$$\delta \mathbf{u}_c^T \mathbf{F} = 0 \quad (24)$$

by definition. Subsequently substituting $\delta \mathbf{u}_c$ for $\delta \mathbf{u}$ in Eq. (23) leads to a set of dynamic equations that are admissible with the constraints yet written in terms of the superfluous set of coordinates. Alternatively, an expression can be developed for \mathbf{F} and substituted in Eq. (23) which can then be solved for any arbitrary $\delta \mathbf{u}$. Such an expression is obtained with the use of Lagrange multipliers [15]:

$$\mathbf{F} = \mathbf{\Gamma}^T \boldsymbol{\lambda} \quad (25)$$

where $\boldsymbol{\lambda}$ is the vector of Lagrange multipliers and $\mathbf{\Gamma}$ is computed from the constraint equations as follows:

$$\mathbf{\Gamma} = \frac{\partial \Phi}{\partial \mathbf{u}} \quad (26)$$

where $\Phi = [\phi_1, \phi_2, \phi_3]^T$ (see Eq. (10)). Substituting Eq. (25) in Eq. (23) and considering $\delta \mathbf{u}$ to be arbitrary leads to the following system of equations:

$$\mathbf{M}\ddot{\mathbf{u}} + \mathbf{V}(\dot{\mathbf{u}}, \mathbf{u}) + \mathbf{G}(\mathbf{u}) - \mathbf{\Lambda}\boldsymbol{\tau} - \mathbf{\Gamma}^T \boldsymbol{\lambda} = \mathbf{0} \quad (27)$$

This system contains 12 equations that must be solved for 15 unknowns (*i.e.* the elements of vectors $\ddot{\mathbf{u}}$ and $\boldsymbol{\lambda}$) in order to simulate the mechanism's dynamics. The remaining three scalar equations that are required are obtained here from the constraint equations expressed at the acceleration level:

$$\mathbf{\Gamma}\ddot{\mathbf{u}} + \dot{\mathbf{\Gamma}}\dot{\mathbf{u}} = \mathbf{0} \quad (28)$$

where the above expression is found by differentiating Eq. (10) twice with respect to time while considering Eq. (26).

The simulation of the mechanism dynamics consists in solving Eqs. (27) and (28) for the coordinate accelerations at a given time instant t_s ($\ddot{\mathbf{u}}_s$) when the coordinate positions and velocities are known for the same time instant (*i.e.* \mathbf{u}_s and $\dot{\mathbf{u}}_s$). Afterwards, the result may be integrated to find $\dot{\mathbf{u}}_{s+1}$ and \mathbf{u}_{s+1} at the subsequent time step t_{s+1} . As noted in [14], any of the available methods will yield an exact value of $\ddot{\mathbf{u}}_s$ if the input values of \mathbf{u}_s and $\dot{\mathbf{u}}_s$ are accurate. However, when the integration is performed, numerical errors may lead to constraint violations. Furthermore, as stated in [16], should the constraints be violated

due to numerical inaccuracy while using velocity or acceleration level constraint equations, the position constraints will cease to be enforceable. A method is thus required to ensure that the coordinate positions and velocities computed during the integration process satisfy the mechanism's constraints. In this work, an approach introduced by Kővecses *et al.* [14] and referred to as the *velocity filtering and configuration corrections* technique is used.

The velocity filtering and configuration corrections technique is based on the decomposition of $\dot{\mathbf{u}}$ into two parts:

$$\dot{\mathbf{u}} = \dot{\mathbf{u}}_v + \dot{\mathbf{u}}_c \quad (29)$$

where $\dot{\mathbf{u}}_v$ is the part of $\dot{\mathbf{u}}$ that is in violation of the constraints while $\dot{\mathbf{u}}_c$ is compatible with them. By multiplying both sides of this equation with $\mathbf{\Gamma}$ and noting that $\mathbf{\Gamma}\dot{\mathbf{u}}_c$, which corresponds to the velocity level constraints (*i.e.* $\partial\Phi/\partial t$) expressed for a compatible set of coordinate velocities, must be zero by definition, the following result is found:

$$\dot{\mathbf{u}}_v = \mathbf{\Gamma}^\dagger \mathbf{\Gamma} \dot{\mathbf{u}} \quad (30)$$

where $\mathbf{\Gamma}^\dagger$ represents a generalized inverse of $\mathbf{\Gamma}$. Moreover, knowing that $\dot{\mathbf{u}}_c$ must be in the nullspace of $\mathbf{\Gamma}$:

$$\dot{\mathbf{u}}_c = (\mathbf{1}_N - \mathbf{\Gamma}^\dagger \mathbf{\Gamma}) \dot{\mathbf{u}} \quad (31)$$

where $\mathbf{1}_N$ is the $N \times N$ identity matrix. In the above decomposition, the following physically-meaningful generalized inverse, based on the use of the generalized inertia matrix as a weighing matrix applied to the norm of $\dot{\mathbf{u}}$, is used [14]:

$$\mathbf{\Gamma}^\dagger = \mathbf{M}^{-1} \mathbf{\Gamma}^T (\mathbf{\Gamma} \mathbf{M}^{-1} \mathbf{\Gamma}^T)^{-1} \quad (32)$$

Based on the above decomposition, it becomes possible to filter from the solution of $\dot{\mathbf{u}}_{s+1}$ obtained by the integration of $\ddot{\mathbf{u}}_s$ the part that violates the constraints. This ensures that the latter will be satisfied at the velocity level. On the other hand, when \mathbf{u}_{s+1} is computed by time integration, it can generally be assumed that it will be in violation of the position level constraints (*i.e.* $\Phi \neq \mathbf{0}$). In order to obtain a set of position coordinates which is compatible with the constraints, it is suggested in [14] to use the following open-loop iterative correction scheme:

$$\mathbf{u}_{s+1}^{\sigma+1} = \mathbf{u}_{s+1}^\sigma - \mathbf{\Gamma}^\dagger(\mathbf{u}_{s+1}^\sigma) \Phi^\sigma \quad (33)$$

where the index σ represents the current iteration and $\mathbf{\Gamma}^\dagger(\mathbf{u}_{s+1}^\sigma)$ is the generalized inverse of $\mathbf{\Gamma}$ evaluated at \mathbf{u}_{s+1}^σ . By using this correction scheme for a preselected number of iterations, the geometrical constraints at the position level are adequately satisfied. The following steps illustrate the detailed process for the dynamic simulation of the tensegrity mechanism:

1. Eqs. (27) and (28) are solved for time step t_s to yield $\ddot{\mathbf{u}}_s$ assuming that $\dot{\mathbf{u}}_s$ and \mathbf{u}_s are known accurately.
2. Using time integration, $\dot{\mathbf{u}}_{s+1}$ is computed.
3. Velocity filtering is used in order to eliminate the part of $\dot{\mathbf{u}}_{s+1}$ that is violating the velocity level constraints: $\dot{\mathbf{u}}_{s+1} = [\mathbf{1}_N - \mathbf{\Gamma}(\mathbf{u}_s)^\dagger \mathbf{\Gamma}(\mathbf{u}_s)] \dot{\mathbf{u}}_{s+1}$.
4. Using time integration, \mathbf{u}_{s+1} is computed.
5. Velocity filtering is used a second time with the updated position coordinates of time t_{s+1} : $\dot{\mathbf{u}}_{s+1} = [\mathbf{1}_N - \mathbf{\Gamma}(\mathbf{u}_{s+1})^\dagger \mathbf{\Gamma}(\mathbf{u}_{s+1})] \dot{\mathbf{u}}_{s+1}$.
6. The configuration corrections scheme (Eq. 33) is applied to \mathbf{u}_{s+1} for 10 iterations.

In the following section, since it is desired to analyze the behaviour of the mechanism while it is being displaced between two equilibrium configurations, the simulation is performed by imposing a trajectory in the actuator space (*i.e.* $\boldsymbol{\psi}$, $\dot{\boldsymbol{\psi}}$ and $\ddot{\boldsymbol{\psi}}$ are provided). It is thus assumed that the corresponding actuator torques could be computed and then be used to generate the same trajectory. However, the simulation of the mechanism with a trajectory imposed in the actuator space requires modifications to be made to the general simulation process described in the previous section. In fact, since $\boldsymbol{\psi}$ and its derivatives are now imposed, only the portion of the dynamic model associated to vector \boldsymbol{q} need to be considered (see Eq. (22)). Eqs. (31) and (33), which are used during the simulation to ensure the satisfaction of the geometrical constraints, must also be modified accordingly. The geometrical constraints expressed at the velocity level can be expressed as:

$$\boldsymbol{\Gamma}\dot{\boldsymbol{u}} = [\boldsymbol{\Gamma}_q, \boldsymbol{\Gamma}_\psi] \begin{bmatrix} \dot{\boldsymbol{q}} \\ \dot{\boldsymbol{\psi}} \end{bmatrix} = \mathbf{0} \quad (34)$$

The value of $\dot{\boldsymbol{q}}$ which satisfies these constraints for a given $\dot{\boldsymbol{\psi}}$ can be computed as follows:

$$\dot{\boldsymbol{q}}_c = (\mathbf{1}_N - \boldsymbol{\Gamma}_q^\dagger \boldsymbol{\Gamma}_q) \dot{\boldsymbol{q}} - \boldsymbol{\Gamma}_q^\dagger \boldsymbol{\Gamma}_\psi \dot{\boldsymbol{\psi}} \quad (35)$$

where:

$$\boldsymbol{\Gamma}_q^\dagger = \mathbf{M}_q^{-1} \boldsymbol{\Gamma}_q^T (\boldsymbol{\Gamma}_q \mathbf{M}_q^{-1} \boldsymbol{\Gamma}_q^T)^{-1} \quad (36)$$

with \mathbf{M}_q being the portion of \mathbf{M} associated to vector \boldsymbol{q} . Finally, Eq. (33) is simply replaced by:

$$\boldsymbol{q}_{s+1}^{\sigma+1} = \boldsymbol{q}_{s+1}^\sigma - \boldsymbol{\Gamma}_q^\dagger (\boldsymbol{u}_{s+1}^\sigma) \boldsymbol{\Phi}^\sigma \quad (37)$$

4.2 Example

In the following, the results of a simulation of the spatial 3-DOF tensegrity mechanism's dynamics using the model developed in Section 3 are presented. From these results, certain observations pertaining to the mechanism's behaviour can be made.

4.2.1 Results

The parameters of the mechanism used for the simulation are: $m = 2.5$, $K = 1000$, $c_d = 100$, $L = \sqrt{2}/2$ and $L_s = \sqrt{2}$. It should be noted here that L_s needs to be chosen while considering the range required for lengths ρ_i . Situations where θ_i approaches 0 or π should also be avoided if possible since in such situations the relation between θ_i and ρ_i is poorly conditioned.

The trajectory imposed, which starts from a reference configuration where $\boldsymbol{\psi}_0 = [-90, -90, -90]^T$ degrees and $\boldsymbol{x}_0 = [\sqrt{2}/4, \sqrt{6}/12, \sqrt{30}/3]^T$ and brings the mechanism to a configuration defined by $\boldsymbol{\psi}_F = [-70.55, -97.13, -84.01]^T$ degrees and $\boldsymbol{x}_F = [1, \sqrt{6}/12, \sqrt{30}/3]^T$, is defined as:

$$\theta_i = \theta_{i_0} - \left(\frac{\theta_{i_F} - \theta_{i_0}}{2} \right) \left\{ \cos \left[\left(\frac{t - t_0}{t_F - t_0} \right) \pi \right] - 1 \right\}, \quad t_0 \leq t \leq t_F \quad (38)$$

with $t_0 = 1$ and $t_F = 3$. The imposed velocity and acceleration trajectories ($\dot{\theta}_i$ and $\ddot{\theta}_i$) are obtained simply by differentiating Eq. (38) with respect to time. The resulting movement of the mechanism's end-effector (*i.e.* the geometric centre of nodes C_i) as represented by the elements of \boldsymbol{x} is shown in Figure 3. Moreover, the variation of the constraint equation values (ϕ_i) along the trajectory are illustrated in Figure 4.

4.2.2 Discussion

In order to generate the results of the previous section, an actuator trajectory was imposed to the mechanism. Although this was done by choice in order to observe the mechanism as it is being displaced from one equilibrium configuration to another, it has been found to be very difficult to simulate the

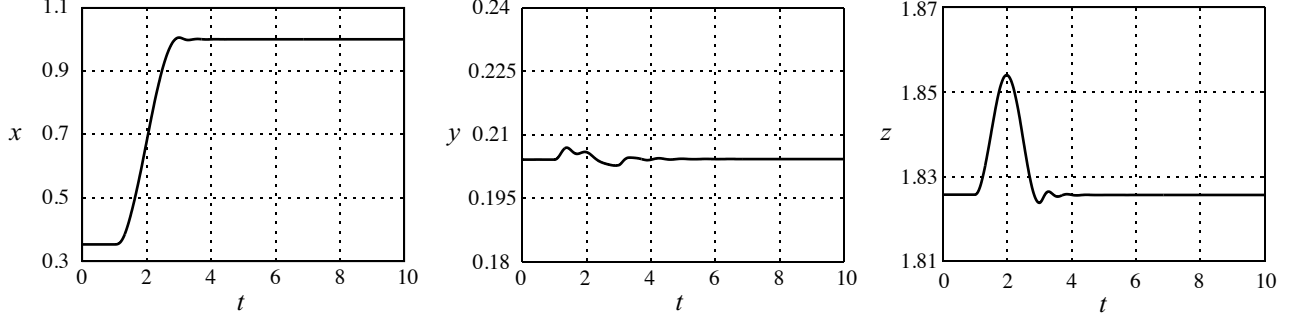


Figure 3: Coordinates x , y and z as a function of time for the simulation trajectory.

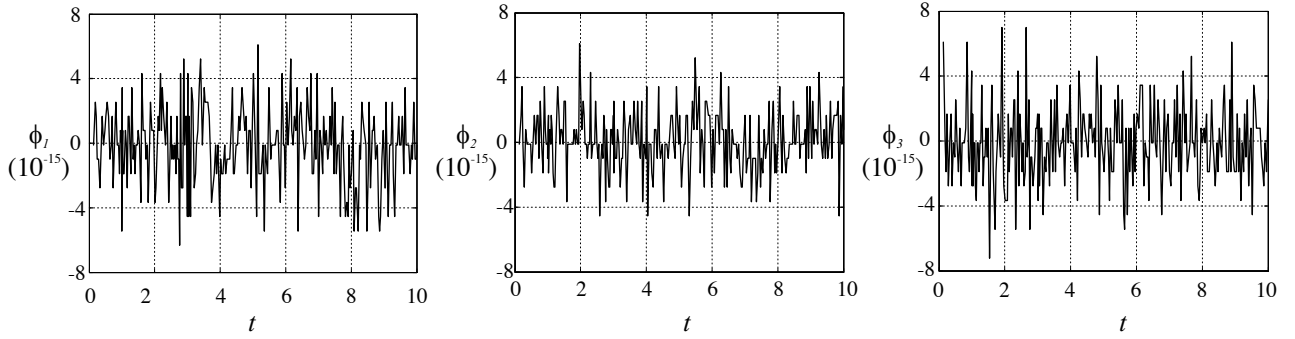


Figure 4: Constraints ϕ_i as a function of time for the simulation trajectory.

mechanism's dynamics while instead providing it with the actuator torques. This is explained in the following.

Although it will not be shown here due to space constraints, it can be demonstrated that, assuming the use of a regular prismatic actuator as the compression component joining nodes A_i and C_i (see Section 2), the amplitude of the compression force acting on this actuator at equilibrium in the absence of external and gravitational loads is $f_i = 2K\rho_i$. Referring to Eq. (1) and Figure 1b, this force can be transformed to the following torque acting on the revolute actuator:

$$\tau_i = K\rho_i\sqrt{4L_s^2 - \rho_i^2} \quad (39)$$

where the square root is always taken as positive. Differentiating τ_i with respect to ρ_i yields:

$$\frac{d\tau_i}{d\rho_i} = \frac{2K(2L_s^2 - \rho_i^2)}{\sqrt{4L_s^2 - \rho_i^2}} \quad (40)$$

It can easily be observed from this equation that the derivative of τ_i with respect to ρ_i is positive when $\rho_i < \sqrt{2}L_s$. Combining this fact with Eq. (1), the following statements can be made:

$$\frac{d\tau_i}{d\rho_i} < 0 \quad \text{if } 0 \leq \theta_i < \pi/2 \quad , \quad \frac{d\tau_i}{d\rho_i} > 0 \quad \text{if } \pi/2 < \theta_i \leq \pi \quad , \quad \frac{d\tau_i}{d\rho_i} = 0 \quad \text{if } \theta_i = \pi/2 \quad (41)$$

where θ_i is restricted between 0 and π by definition. Suppose that the mechanism is initially in equilibrium at a configuration with a given set of actuator positions. Suppose next, without loss of generality, that the mechanism must be displaced to a new equilibrium by increasing ρ_1 by an infinitesimal amount. If θ_1

is located between 0 and $\pi/2$ in the initial configuration, it can be observed from Eq. (41) that the slight increase in ρ_1 will lead to a corresponding decrease in τ_1 . The actuator torque τ_1 required at the new equilibrium is thus smaller than the one required in the initial configuration. However, in order to allow ρ_1 to increase, τ_1 must also be initially increased above its original value to provide the supplementary force required to further separate nodes A_i and C_i and, correspondingly, to raise the amount of potential energy stored in the mechanism's springs. This initial increase and subsequent decrease of τ_1 (or vice-versa) also occurs in other systems (*e.g.* the inverted pendulum). However, it seems as though the presence of unconstrained degrees of freedom in tensegrity mechanisms makes them more susceptible to numerical errors during the simulation process. When such errors are combined with the behaviour described above, the result is usually an eventual collapse of the mechanism.

From Figure 3, it can be observed that once ψ_F ($t = 3$) has been reached, there is a delay before the mechanism settles in its new equilibrium (\mathbf{x}_F). This is due to the unconstrained degrees of freedom which are influenced only by the mechanism's dynamic properties and by the imposed trajectory. In an application where the mechanism would be driven by imposing the actuator torques with a Cartesian-based control system, this delay could potentially be reduced.

It can also be seen from Figure 3 that the mechanism is underdamped in spite of the relatively high damping coefficient that was used during the simulation. This poor transformation from damping to actual energy dissipation has been previously documented for some tensegrity systems [17]. For the mechanism studied here, the low energy dissipation is due in large part to the geometrical arrangement of the damped elements with respect to the unconstrained degrees of freedom. One feasible solution to this problem would be to use linear dampers to create rotational damping in the mechanism's universal joints. The energy dissipating contribution of the universal joints' natural damping can also be considered.

Finally, from Figure 4, it can be observed that the constraints (Eq. (10)) are satisfied to the order of 10^{-15} throughout the entire trajectory. Although it isn't shown, the velocity level constraints, for their part, were satisfied to the order of 10^{-5} . This demonstrates the efficiency of the velocity filtering and configuration corrections method [14].

5 Conclusion

In this paper, the dynamics of a novel spatial 3-DOF tensegrity mechanism were analyzed. When in equilibrium, the mechanism is capable of positioning its end-effector in the Cartesian space with the use of three revolute actuators. However, since the mechanism has six unconstrained degrees of freedom, its motion between equilibrium configurations cannot be fully controlled and is largely dictated by its dynamic properties. For this reason, it becomes very important to simulate the mechanism's dynamics in order to study its behaviour.

The equations of motion of the mechanism were first developed using the Lagrangian formulation. As it is the case with parallel mechanisms, it was seen that the tensegrity mechanism is subjected to holonomic nonlinear geometrical constraints. These constraints must thus be considered during the solution to the forward dynamic problem. A new method proposed in [14] which is based on velocity filtering and configuration corrections was used to perform the dynamic simulation. This method was shown to be rather simple to apply while also being very effective in ensuring constraint satisfaction.

Finally, it was stated that the transformation from linear damping in the mechanism's springs to actual energy dissipation is relatively poor. This is due to the geometrical arrangement of the springs relative to the unconstrained degrees of freedom. One possible solution to this problem is to create rotational damping in the mechanism's universal joints by using linear dampers.

Acknowledgements: The authors wish to thank the Natural Sciences and Engineering Research Council of Canada (NSERC) as well as the Fonds Québécois de la Recherche sur la Nature et les Technologies (FQRNT) and the Canada Research Chair Program (CRC) for their financial support.

References

- [1] B. Fuller. *Synergetics: The Geometry of Thinking*. MacMillan Publishing Co., Inc., New York, 1975.
- [2] R. Motro. Tensegrity systems: The state of the art. *International Journal of Space Structures*, 7(2):75–83, 1992.
- [3] M. Arsenault and C. M. Gosselin. Development and analysis of a planar 1-DOF tensegrity mechanism. In *Proceedings of the 2004 Canadian Society of Mechanical Engineering (CSME) Forum*, 2004.
- [4] I. J. Oppenheim and W. O. Williams. Tensegrity prisms as adaptive structures. *ASME Adaptive Structures and Material Systems*, 54:113–120, 1997.
- [5] T. M. Tran. Reverse displacement analysis for tensegrity structures. Master’s thesis, University of Florida, Florida, USA, 2002.
- [6] J. Bayat and C. D. Crane III. Closed-form equilibrium analysis of a planar tensegrity structure. In *Proceedings of the 9th International Symposium on Advances in Robot Kinematics*, 2004.
- [7] M. Q. Marshall and C. D. Crane III. Design and analysis of a hybrid parallel platform that incorporates tensegrity. In *Proceedings of the ASME 2004 Design Engineering Technical Conferences*, 2004.
- [8] C. Sultan and M. Corless. Tensegrity flight simulator. *Journal of Guidance, Control, and Dynamics*, 23(6):1055–1064, 2000.
- [9] C. Sultan, M. Corless, and R. E. Skelton. Peak to peak control of an adaptive tensegrity space telescope. In *Proceedings of SPIE - The International Society for Optical Engineering*, volume 3667, pages 190–201, 1999.
- [10] C. Sultan and R. Skelton. A force and torque tensegrity sensor. *Sensors and Actuators, A: Physical*, 112(2–3):220–231, 2004.
- [11] D.A. Streit and B.J. Gilmore. Perfect spring equilibrators for rotatable bodies. *ASME Journal of Mechanisms, Transmissions, and Automation in Design*, 111(4):451–458, 1989.
- [12] J. Herder. *Energy-Free Systems: Theory, Conception and Design of Statically Balanced Spring Mechanisms*. PhD thesis, Delft University of Technology, Delft, The Netherlands, 2001.
- [13] M. Arsenault and C.M. Gosselin. Static balancing of tensegrity mechanisms. Submitted to the ASME 2005 International Design Engineering Technical Conferences & Computers and Information in Engineering Conference, September 2005.
- [14] J. Kövecses, J.-C. Piedboeuf, and C. Lange. Dynamics modeling and simulation of constrained robotic systems. *IEEE/ASME Transactions of Mechatronics*, 8(2):165–177, 2003.
- [15] R. M. Rosenberg. *Analytical Dynamics of Discrete Systems*. Plenum, New York, 1977.
- [16] X. Yun and N. Sarkar. Unified formulation of robotic systems with holonomic and nonholonomic constraints. *IEEE Transactions on Robotics and Automation*, 14(4):640–650, 1998.
- [17] I. J. Oppenheim and W. O. Williams. Vibration and damping in a three-bar tensegrity structure. *Journal of Aerospace Engineering*, 14(3):85–91, 2001.